Results in Physics 42 (2022) 105972

Contents lists available at ScienceDirect

Results in Physics

journal homepage: www.elsevier.com/locate/rinp

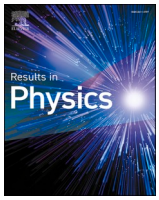

Broadband metamaterial absorber based on hybrid multi-mode resonance in mid-wave and long-wave infrared region

ARTICLE INFO

Keywords
Broadband
Metamaterial absorber
Dual-band
Hybrid multi-mode resonance

ABSTRACT

The infrared radiation of the target and scene needs to be transmitted through the surface atmosphere, and it can be detected by infrared thermal imaging equipment. The mid-wave infrared band (MWIR, 3–5 μm) and the long-wave infrared band (LWIR, 8–14 μm) are two atmospheric windows for heat transmission and are the principal operating band of infrared equipment. This paper proposed a broadband metamaterial absorber based on hybrid multi-mode resonance in the MWIR and LWIR. Metamaterial absorber with rectangular grating structure achieves a total of six absorption peaks with high absorption in the MWIR and LWIR. The proposed absorber is scalability in the MWIR and LWIR by tuning the structural parameters. And we designed six absorption peaks to achieve a broadband absorber based on the combined action of propagating surface plasmons (PSP), localized surface plasmons (LSP), and Fabry–Pérot (FP) resonance modes. The average absorption rate of the MWIR is 52 %, and the average absorption rate of the LWIR is 86 %. The geometry of the absorber structure is relatively large, which facilitates fabrication and integration. Although, in terms of its resonance mechanism, the absorption is directly related to the incident angle. However, the metamaterial absorber maintains good wide-angle characteristics when the incident angle is ± 45°. Therefore, the proposed dual-band absorbers in the MWIR and LWIR will have great application potential in infrared detection devices.

Introduction

As the essential part of infrared equipment, research on high-performance infrared detectors has become the main breakthrough point for advanced infrared imaging systems. And the related research has received extensive attention [1–3]. According to the law of black body radiation, the thermal radiation wavelength of high-temperature objects is in the MWIR band, and the thermal radiation wavelength of normal-temperature objects is in the LWIR band. The operating band of most of the thermal imaging systems includes the MWIR or the LWIR band. For infrared detectors, circuit transmission efficiency, calculation algorithm, absorption efficiency, and absorption spectrum width are used as relevant indicators to measure their performance [4]. Among them, the absorption spectrum width and absorption efficiency are of great significance in the application of the detector. The traditional absorption material is based on the intrinsic absorption of the material itself. So that the absorption efficiency is low, the absorption peak position cannot be changed, and the ability to adjust and design is limited. Achieving high absorption in the infrared band requires a relatively large thickness. The thickness of the structure has excellent limitations for improving the detector's performance and the development of miniaturized and integrated devices.

Due to their flexible design and high absorption, metamaterial absorbers have been widely studied in various fields, such as imaging [5–9], sensing [10,11], and detection [12]. Landy *et al.* designed a split-ring resonator to achieve perfect absorption in the microwave band and first proposed the concept of metamaterial absorbers [13]. Scholars have generated significant interest in metamaterials and carried out a lot of research. To date, metamaterial absorbers have been realized in multiple wavelength bands: microwave [14,15], visible light [16–20], infrared [12,21–23], and terahertz [24–26]. However, there are hardly any relevant research studies on both MWIR and LWIR absorbers presently. Liu *et al.* designed a perfect absorber for infrared metamaterials based on the cross structure, and the experimental results were in good agreement with the numerical full-wave simulations [27]. Duan *et al.* proposed a split-loop resonator array as the top layer pattern and SU8 as the spacer layer material, which can achieve near-unity absorption in the terahertz band. The absorption peak position shifts with the spacer layer thickness [28]. For metal-dielectric-metal (MDM) metamaterial structures, near-unity absorption usually occurs in a very narrow wavelength range determined by the thickness of the dielectric layer [29–31]. The narrowband feature has limitations in some application scenarios. And broadband, multi-band absorbers began to be studied for absorption devices [32]. Broadband or multi-band absorbers can be obtained by designing the top metal structure to use asymmetric or mixed-sized nanostructures to excite multiple resonances [33]. These methods had certain limitations in obtaining dual-band absorbers in MWIR and LWIR bands. A novel absorber in commercial products requires simple fabrication, low cost, and easy integration into existing process lines. Then as the absorber pattern becomes smaller and more complex, so does the fabrication. At the same time, the stability of the incident angle is very important for the application of the device. Therefore, for practical applications, the absorber should be easy to fabricate, have high absorption, broadband absorption characteristics, and good incident angle stability.

This paper proposed a square grating-structured absorber to achieve

https://doi.org/10.1016/j.rinp.2022.105972
Received 28 March 2022; Received in revised form 1 September 2022; Accepted 4 September 2022
Available online 8 September 2022

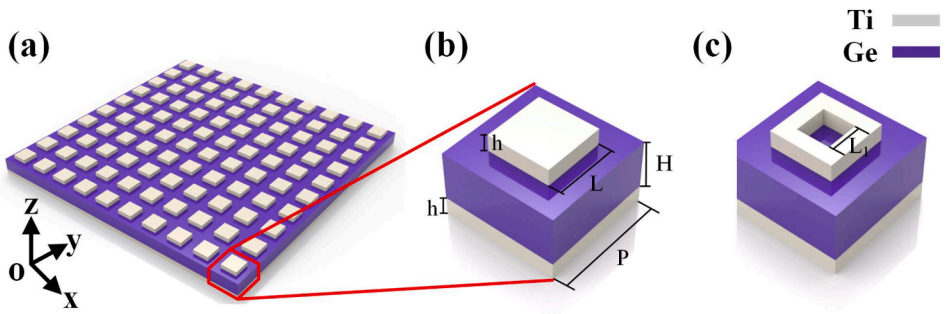

Fig. 1. Schematic diagram of the rectangular grating metamaterial absorber: (a) the periodic array structure, (b) the rectangular cell structure, (c) the rectangular closed-loop cell structure.

broadband absorption in the MWIR and LWIR. The absorber could simultaneously absorb the thermal radiation energy of high-temperature and normal-temperature objects, increasing the applicability of applications. At the same time, increasing the detection object information can reduce the detection false alarm rate. The proposed rectangular grating metamaterial absorber structure was designed to excite a variety of electromagnetic resonance modes and achieve two absorption peaks in the MWIR and four absorption peaks in the LWIR, respectively. The design integrated six absorption peaks to achieve broadband absorption of the MWIR and LWIR. The absorber exhibited an average absorption rate of 52 % in the MWIR (3.3–4.4 μm) and 86 % in the LWIR (8.5–12.5 μm). By revealing the mechanism and principle of realizing broadband absorption in the MWIR and LWIR, the excitation of FP resonance mode, PSP and LSP resonance mode in the Ti/Ge/Ti three-layer absorber was analyzed. The hybrid-mode and broadband absorption performance could be tuned by changing the geometric parameters of the proposed structure. The relevant structural parameters of the absorber were analyzed in this paper. At the same time, the structure has a relatively large structure size, which can facilitate batch fabrication. And for the requirements of high angular stability characteristics of the infrared detection device, the absorber can also meet the requirements. These characteristics have outstanding advantages in infrared imaging, detection, and other fields.

Design and results

Metamaterial absorbers with unique physical properties and near-unity absorption rates have recently received extensive attention. A broadband absorber structure is proposed based on multi-mode resonance in the MWIR and LWIR regions. The proposed MDM absorber is shown in Fig. 1: the Ti rectangular grating array is placed on top, and a Ti plane layer separated by dielectric Ge is placed on the bottom. The thickness of the Ti film is 0.1 μm, which is greater than the skin depth in the infrared band. The elimination of infrared radiation transmittance is achieved, and the transmission is 0. And Ti can also be used as a heat transfer dielectric in infrared detector applications. Ti has a higher loss than metals such as gold and silver, and the bandwidth of the absorption peak is relatively more expansive, which is also the reason for choosing the metal Ti. As a dielectric material with a relatively large refractive index in the infrared band, Ge is a suitable choice for the design of multi-mode resonance. The design idea of metamaterial absorbers is to reduce transmission and reflection to achieve high absorption. According to the equivalent dielectric theory, these absorbers based on sub-wavelength structural units can be equivalent dielectrics. The absorber impedance (Z) and free space impedance (Z_0) can be matched through the practical design of structural parameters. The following equation gives the relation:

$$A(\lambda) = 1 - R(\lambda) = 1 - \left|\frac{Z - Z_0}{Z + Z_0}\right|^2 = 1 - \left|\frac{Z_{eff} - 1}{Z_{eff} + 1}\right|^2 \quad (1)$$

where A(λ) and R(λ) are the absorber structure's absorption and reflection at wavelength λ, respectively, and Z_{eff} is the equivalent relative impedance. The absorber structure is designed based on the finite-difference time-domain (FDTD) method. Periodic boundary conditions were applied in both the x and y directions, while the perfectly matched-layer (PML) boundary condition was applied in the z direction (electromagnetic waves propagation). Normally incident TM plane wave was used to excite the square grating-structured absorber. The optical constants of Ti and Ge used in the calculation were extracted from the data reported by Palik [34,35]. The absorber array is shown in Fig. 1(a). By designing the surface Ti square with a side length L of 3.5 μm, the dielectric Ge thickness H of 0.6 μm, and the period P of 6.8 μm, the absorber achieved impedance matching (shown in Fig. 2(b)). And the result of high broadband absorption in the MWIR and LWIR was

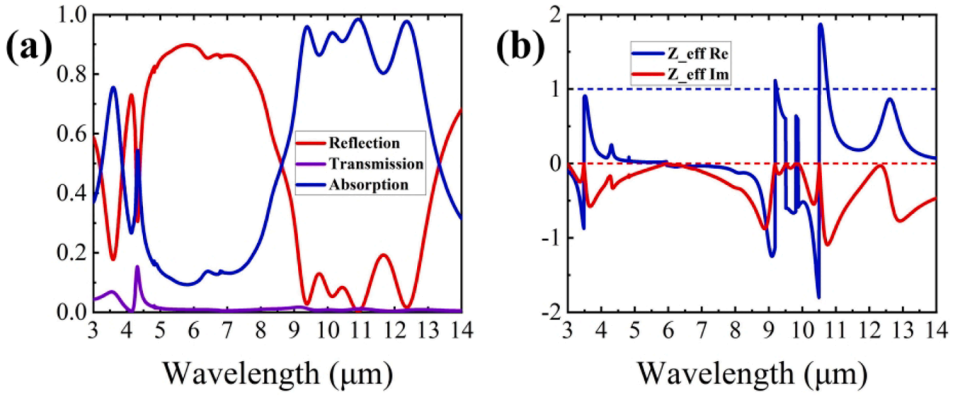

Fig. 2. (a) The absorption, reflection, and transmission spectra line of rectangular grating absorbers. (b) The real and imaginary parts of the equivalent impedance of the rectangular grating absorbers. The geometric parameters: h = 0.1 μm, H = 0.6 μm, L = 3.5 μm and P = 6.8 μm.

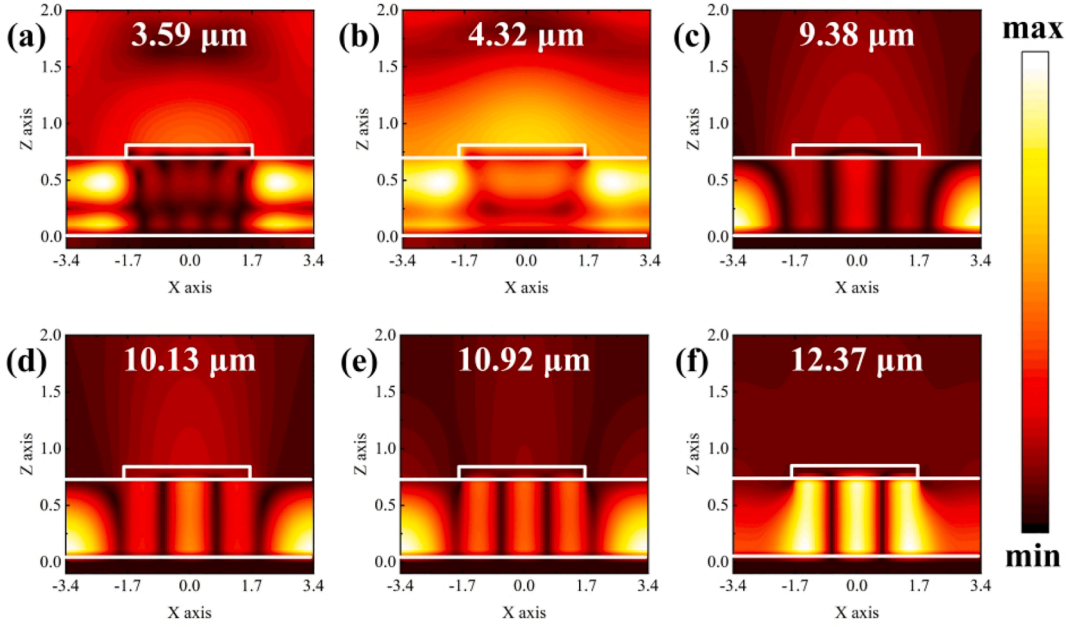

Fig. 3. The magnetic field distribution of the six absorption peak positions of the absorber.

achieved. Fig. 1(c) shows a rectangular closed-loop cell structure, where L_1 is the inner side length. The effect of L_1 on the absorption characteristics of the absorber is discussed in the following section 3.2.

By calculating the absorption characteristics of the absorber structure based on the FDTD method for the above design, the reflection, transmission, and absorption spectrum of the absorber is shown in Fig. 2 (a). The single-size rectangular grating array structure realizes six absorption peaks in the MWIR: 3.59 μm, 4.32 μm, and the LWIR: 9.38 μm, 10.13 μm, 10.92 μm, 12.37 μm, and the absorption rates are 76 %, 55 %, 96 %, 94 %, 98 %, 98 %. The average absorption rate of the MWIR (3.3–4.4 μm) is 52 %, and the average absorption rate of the LWIR (8.5–12.5 μm) is 86 %. Although the absorption of the MWIR is relatively low, it can meet the application requirements. Based on the S-parameter inversion method for the equivalent dielectric theory [36–38], the equivalent relative impedance Z_{eff} of the absorber structure is analyzed, and the equation is as follows:

$$Z_{eff} = \sqrt{\frac{(1+S_{11})^2 - S_{21}^2}{(1+S_{11})^2 + S_{21}^2}} \tag{2}$$

The real and imaginary parts of the equivalent relative impedance were obtained by calculation, as shown in Fig. 2(b). It can be seen from Equation (1) that impedance matching is achieved when the real part is equal to 1 and the imaginary part is equal to 0. The six absorption peaks in the absorption spectrum of Fig. 2(a) correspond to the six mode points in Fig. 2(b). Impedance matching reflects the absorption efficiency of the absorber. The higher the degree of matching, the higher the absorption rate. In addition, the equivalent medium calculated by the S-parameter inversion method may be affected by the resonant mode and the FDTD approximation algorithm, such as PSP resonance. Therefore, all factors mentioned above lead to Fig. 2(b).

Discussion

Absorption mechanism analysis

To further understand the reason for the absorption spectrum, we analyzed the magnetic field strength distribution at the six absorption peak positions in the absorption spectrum. As shown in Fig. 3, the magnetic field distribution of the six absorption peaks indicated the physical mechanism of each absorption peak. The magnetic field distribution at 9.38 μm in LWIR was mainly concentrated in the dielectric between adjacent rectangular structures, as shown in Fig. 3(c). In contrast, it was also observed from Fig. 3(f) that the magnetic field at 12.37 μm was mainly concentrated in the dielectric layer directly below

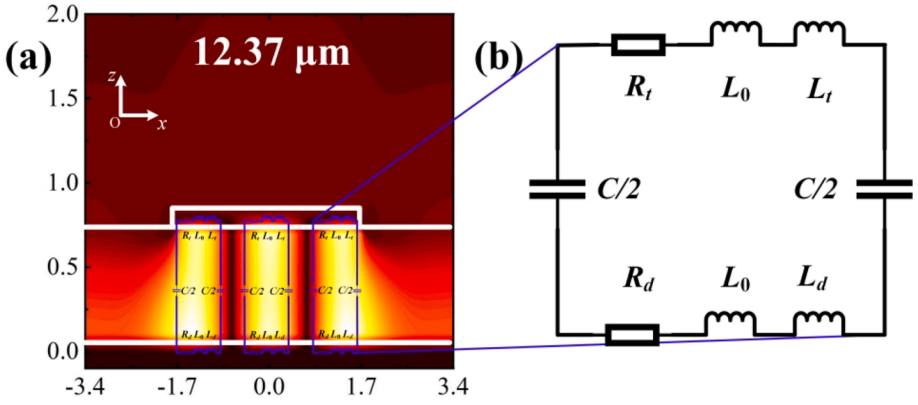

Fig. 4. The RLC circuit models of the third-order LSP resonance mode at a resonance wavelength of 12.37 μm.

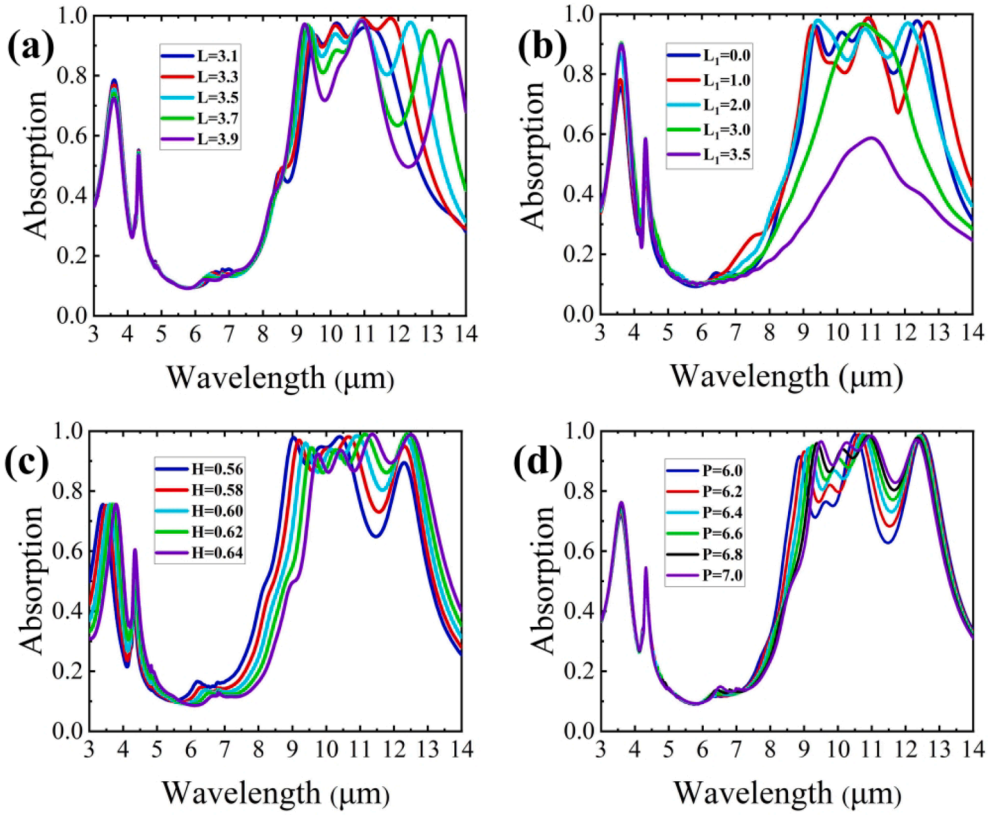

Fig. 5. The influence on the absorption line of (a) the side length L of the rectangular grating cell structure, (b) the inner side length L_1 of the square closed-loop structure, (c) the dielectric thickness H, and (d) the period P of the array with basic dimensions h = 0.1 μm, H = 0.6 μm, L = 3.5 μm, and P = 6.8 μm.

the rectangular grating. And the magnetic field in the dielectric was divided into three parts. It can be known that the two absorption peaks are generated by the excitation of the PSP (Fig. 3(c)) and the third-order LSP (Fig. 3(f)), respectively. The relation between the PSP wavelength λ_{PSP} and period P could be explained by the PSP dispersion relationship, given by the following equation [39]:

$$\lambda_{PSP} = \frac{\mathrm{P}}{\sqrt{\mathrm{i}^2 + \mathrm{j}^2}} \sqrt{\frac{\varepsilon_\mathrm{d}\varepsilon_\mathrm{m}}{\varepsilon_\mathrm{d} + \varepsilon_\mathrm{m}}} \tag{3}$$

where ε_m and ε_d represent the permittivity of metal Ti and dielectric Ge, and i and j are integers. And the LSP mode can be explained by the equivalent circuit theory. A resistor-inductor-capacitor (RLC) circuit model of the third-order LSP resonance was developed, as shown in Fig. 4(a). L_0 is the inductance of two parallel plates separated by a dielectric spacer. R_t and L_t are the resistance and inductance of the top structure, respectively. R_b and L_b are the resistance and inductance of the bottom metal, respectively. The capacitance of the dielectric space between the two metal layers is C, and there is no capacitance between adjacent cell structures. According to the RF circuit resonance analysis method [40], the parameters of the RLC circuit model shown in Fig. 4(b) can be obtained as follows:

$$L_0 = \frac{\mu_0 \mathrm{h}}{6} \tag{4}$$

$$C = \frac{2\beta\varepsilon_0\varepsilon_\mathrm{d}\mathrm{L}^2}{3\mathrm{h}} \tag{5}$$

$$R_t = \frac{1}{3\delta_{eff}\omega\varepsilon_0}\left(\frac{\varepsilon_2}{\varepsilon_1^2+\varepsilon_2^2}\right) \tag{6}$$

$$R_b = \frac{1}{3\delta_{eff}\omega\varepsilon_0}\left(\frac{\varepsilon_2}{\varepsilon_1^2+\varepsilon_2^2}\right) \tag{7}$$

$$L_t = \frac{-1}{3\delta_{eff}\omega^2\varepsilon_0}\left(\frac{\varepsilon_1}{\varepsilon_1^2+\varepsilon_2^2}\right) \tag{8}$$

$$L_b = \frac{-1}{3\delta_{eff}\omega^2\varepsilon_0}\left(\frac{\varepsilon_1}{\varepsilon_1^2+\varepsilon_2^2}\right) \tag{9}$$

where ω is the angular frequency of the incident light, μ_0 and ε_0 are the vacuum permeability and permittivity, respectively. ε_1 and ε_2 are the real and imaginary parts of the permittivity ε_m of metallic Ti. β considers the non-uniform charge distribution along the surfaces of the capacitor. δ_{eff} is the effective power penetration depth of metal Ti. The resonance wavelength can be expressed as.

$$\lambda_{LSP} = 2\pi cC\sqrt{2L_0 + L_t + L_b} \tag{10}$$

In addition, Fig. 3(a) shows the absorption peak at 3.59 μm in the MWIR was from the high-order FP resonance of the dielectric Ge. The absorption peaks at 10.13 μm and 10.92 μm are due to the combined effect of mixed first-order FP resonance, PSP resonance, and third-order LSP resonance, as shown in Fig. 3(d) and Fig. 3(e). The above theoretical analysis also reflects the importance of Ge in the design. Finally, at 4.32 μm in Fig. 3(b), it was related to the specific dielectric properties of metallic Ti. It was also seen from the transmission curve in Fig. 2(a) that there is a particular transmission at 4.32 μm, which is also for this reason.

Size modulation analysis

The properties of metamaterial absorbers mainly depended on the feature size of the structural units. The MDM absorber's resonance

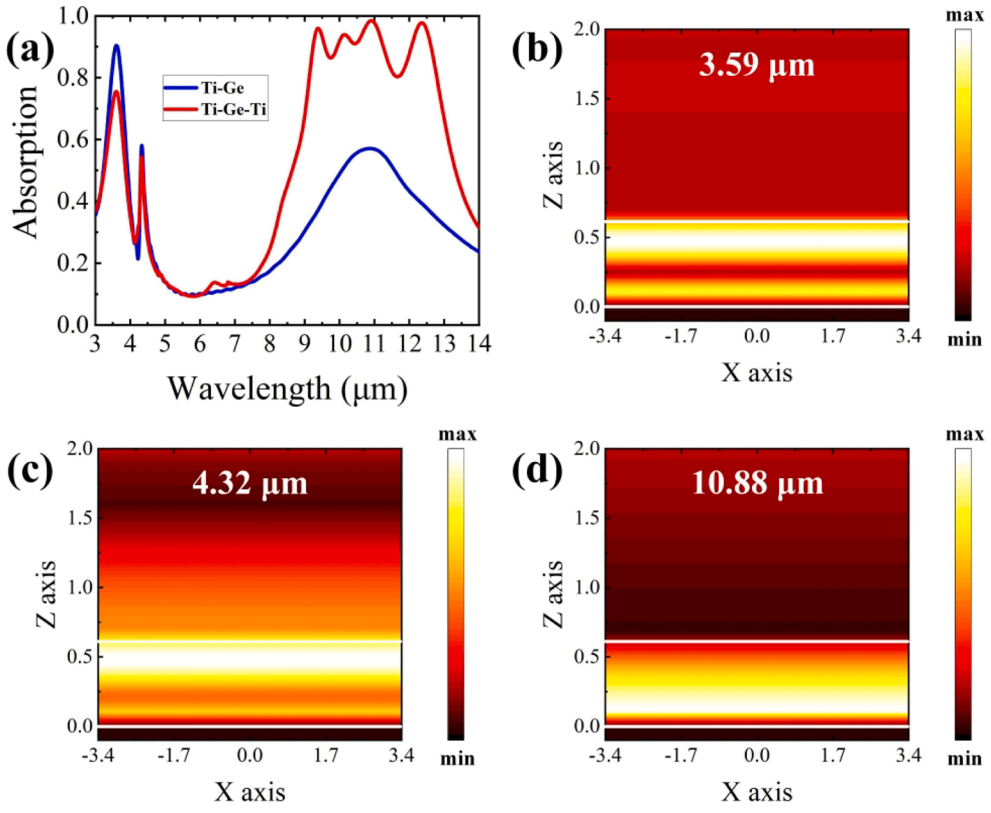

Fig. 6. (a) The comparison of the absorption situation without the top structure (bottom Ti h = 0.1 μm and Ge H = 0.6 μm), and (b) (c) (d) the magnetic field distribution at the position of the absorption peak.

wavelength λ and absorption could be tuned by changing the array period P, pattern side length L, dielectric layer thickness H, and the inner side length of the rectangular box L_1, respectively. Fig. 5 shows the absorption spectrum changes by changing the relevant parameters when the basic structure parameters are L = 3.5 μm, L_1 = 0 μm, P = 6.8 μm, and H = 0.60 μm. Fig. 5(a) shows the absorption spectrum change with the evolution of the length L of the square side of the surface. During the side length L transition from 3.1 μm to 3.9 μm, the third-order LSP absorption peak in the LWIR is redshift; the absorption of the MWIR and the FP resonance absorption peak in the LWIR decreased. This phenomenon is because the increase of L affects the energy of the light incident into the FP cavity. Fig. 5(b) shows the variation of the absorption spectra line with the change of L_1 in the rectangular box structure (Fig. 1(c)). As L_1 became more extensive, the absorption of the absorption peak of MWIR at 3.59 μm became larger. When L_1 was 3.5 μm, it was the absorption without a surface pattern. The effect of the dielectric layer thickness on the absorption spectrum is shown in Fig. 4 (c). As the dielectric layer thickness increased from 0.56 μm to 0.64 μm, the FP resonance absorption peak was redshift, and the plasmon resonance matching conditions changed, resulting in an expected result. Fig. 5(d) shows the effect of period P variation on absorption. The absorption at 12.37 μm in the LWIR and 4.32 μm in the MWIR did not change as the period varied from 6 μm to 7 μm. And with the increase of the period P, the resonance peak of the PSP underwent a redshift. At the same time, the FP resonance absorptivity increased due to the increase of the energy of the incident light of the unit structure.

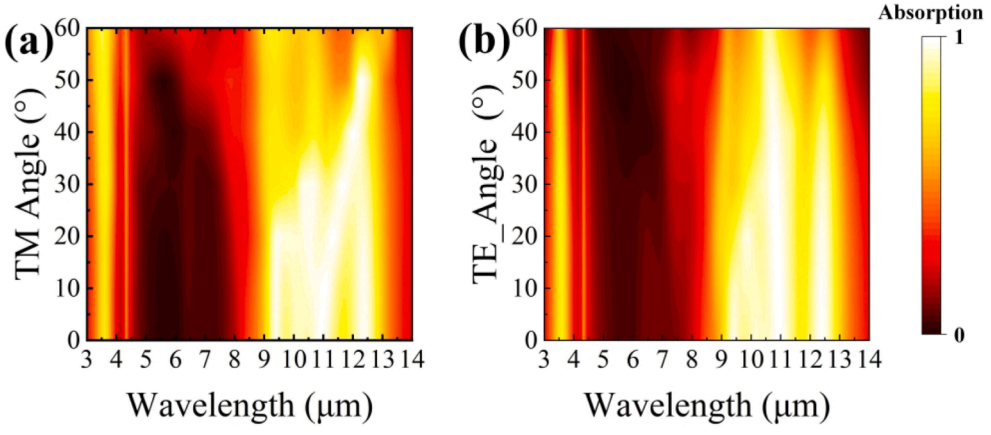

Fig. 7. The influence of the incident angle on absorption under the TM and TE modes.

No top-layer partner structural analysis

To deepen the understanding of the absorber structure, we compared the absorption spectra lines with and without the surface pattern structure shown in Fig. 6(a). When L_1 is equal to 3.5 μm, that is, there is no surface pattern structure. The magnetic field distribution at the three absorption peaks in the MWIR and LWIR were analyzed. It was seen from Fig. 6(a) that when there was no surface pattern, the absorption peak at 3.59 μm in the MWIR became stronger due to the increase in the amount of incident light. It was also seen in Fig. 6(b) and Fig. 6(d) that the magnetic field intensity distribution of the FP resonance could be seen in the dielectric. They were the high-order FP resonance mode at 3/4 wavelength and the intrinsic FP resonance mode at 1/4 wavelength, respectively. The absorption at 4.32 μm was mainly based on a specific dielectric constant singularity in the metal Ti, resulting in an abnormal transmission and absorption.

Impact of the incidence angle on absorption

Omnidirectional or wide-angle absorption is ideal for infrared detection devices to ensure efficient light collection. We investigated the optical properties of the rectangular grating absorber under different incidence angles of transverse magnetic polarized light (TM) and transverse electric polarized light (TE). As shown in Fig. 7, we can see that during the change of the incident angle from 0° to 60° in the two modes, the near-perfect absorption still exists in a wide range of incident angles. Although the FP resonance mode and the propagating plasmon mode were related to the incident angle, from the results, the absorber still had good absorption characteristics in the range of ± 45°, indicating that the absorber had a good incidence angular stability.

Conclusion

In general, to meet the detection requirements of the atmospheric window in the infrared band, we designed a broadband absorber that responds simultaneously in the MWIR and LWIR. The absorber had a relatively large feature size and was easy to process. It achieved six absorption peaks in the MWIR and LWIR, while the average absorption rate of the MWIR is 52 %, and the average absorption rate of the LWIR is 86 %. The modulation of the characteristic absorption peaks could be achieved by adjusting the relative feature size of the rectangular grating array. The reason and physical mechanism of the absorption were explained by analyzing the magnetic field with or without the surface square structure. Finally, the wide-angle characteristics of the absorber were calculated, and the results showed that the absorber had good incident angle stability and maintained good absorption characteristics within the range of the incident angle ± 45°. The design of the broadband absorber structure in the MWIR and LWIR provides a new research direction for infrared detection devices.

Funding

This work was funded by the National Natural Science Foundation of China (61735018, 61805242); Scientific and Technological Development Project of Jilin Province (20220201080GX); Excellent Member of Youth Innovation Promotion Association of the Chinese Academy of Sciences (2014193, Y201836); Leading Talents and Team Project of Scientific and Technological Innovation for Young and Middle-aged Groups in Jilin Province (20190101012JH).

Declaration of Competing Interest

The authors declare that they have no known competing financial interests or personal relationships that could have appeared to influence the work reported in this paper.

Data availability

No data was used for the research described in the article.

References

[1] Suen JY, Fan K, Montoya J, Bingham C, Stenger V, Sriram S, et al. Multifunctional metamaterial pyroelectric infrared detectors. Optica 2017;4.
[2] Dao TD, Ishii S, Yokoyama T, Sawada T, Sugavaneshwar RP, Chen K, et al. Hole Array Perfect Absorbers for Spectrally Selective Midwavelength Infrared Pyroelectric Detectors. ACS Photonics 2016;3:1271–8.
[3] Livache C, Martinez B, Goubet N, Greboval C, Qu J, Chu A, et al. A colloidal quantum dot infrared photodetector and its use for intraband detection. Nat Commun 2019;10:2125.
[4] Jalil SA, Lai B, ElKabbash M, Zhang J, Garcell EM, Singh S, et al. Spectral absorption control of femtosecond laser-treated metals and application in solar-thermal devices. Light Sci Appl 2020;9:14.
[5] Zhang Y, Min C, Dou X, Wang X, Urbach HP, Somekh MG, et al. Plasmonic tweezers: for nanoscale optical trapping and beyond. Light Sci Appl 2021;10:59.
[6] Hong J, Son H, Kim C, Mun SE, Sung J, Lee B. Absorptive metasurface color filters based on hyperbolic metamaterials for a CMOS image sensor. Opt Express 2021;29:3643–58.
[7] Xuan Z, Li J, Liu Q, Yi F, Wang S, Lu W. Artificial Structural Colors and Applications. Innovation 2021;2(1):100081.
[8] Plidschun M, Ren H, Kim J, Forster R, Maier SA, Schmidt MA. Ultrahigh numerical aperture meta-fibre for flexible optical trapping. Light Sci Appl 2021;10:57.
[9] Xu HX, Hu G, Wang Y, Wang C, Wang M, Wang S, et al. Polarization-insensitive 3D conformal-skin metasurface cloak. Light Sci Appl 2021;10:75.
[10] Palermo G, Lio GE, Esposito M, Ricciardi L, Manoccio M, Tasco V, et al. Biomolecular Sensing at the Interface between Chiral Metasurfaces and Hyperbolic Metamaterials. ACS Appl Mater Interfaces 2020;12:30181–8.
[11] Liao YL, Zhao Y. Ultra-narrowband dielectric metamaterial absorber with ultra-sparse nanowire grids for sensing applications. Sci Rep 2020;10:1480.
[12] Wei J, Xu C, Dong B, Qiu CW, Lee C. Mid-infrared semimetal polarization detectors with configurable polarity transition. Nat Photonics 2021;15:614–21.
[13] Landy NI, Sajuyigbe S, Mock JJ, Smith DR, Padilla WJ. Perfect metamaterial absorber. Phys Rev Lett 2008;100:207402.
[14] Rao JW, Zhao YT, Gui YS, Fan XL, Xue DS, Hu CM. Controlling Microwaves in Non-Hermitian Metamaterials. Phys Rev Appl 2021;15.
[15] Qu S, Hou Y, Sheng P. Conceptual-based design of an ultrabroadband microwave metamaterial absorber. Proc Natl Acad Sci USA 2021;118.
[16] Dixon K, Montazeri AO, Shayegannia M, Barnard ES, Cabrini S, Matsuura N, et al. Tunable rainbow light trapping in ultrathin resonator arrays. Light Sci Appl 2020;9:194.
[17] Xu B, Li H, Gao S, Hua X, Yang C, Chen C, et al. Metalens-integrated compact imaging devices for wide-field microscopy. Adv Photonics 2020;2.
[18] Jiang T, Li C, He Q, Peng ZK. Randomized resonant metamaterials for single-sensor identification of elastic vibrations. Nat Commun 2020;11:2353.
[19] Song Q, Baroni A, Wu PC, Chenot S, Brandli V, Vezian S, et al. Broadband decoupling of intensity and polarization with vectorial Fourier metasurfaces. Nat Commun 2021;12:3631.
[20] Qu G, Yang W, Song Q, Liu Y, Qiu CW, Han J, et al. Reprogrammable meta-hologram for optical encryption. Nat Commun 2020;11:5484.
[21] Ruan X, Dai W, Wang W, Ou C, Xu Q, Zhou Z, et al. Ultrathin, broadband, omnidirectional, and polarization-independent infrared absorber using all-dielectric refractory materials. Nanophotonics 2021;10:1683–90.
[22] Wang Y, Chen Q, Yang W, Ji Z, Jin L, Ma X, et al. High-efficiency broadband achromatic metalens for near-IR biological imaging window. Nat Commun 2021;12:5560.
[23] Lei L, Li S, Huang H, Tao K, Xu P. Ultra-broadband absorber from visible to near-infrared using plasmonic metamaterial. Opt Express 2018;26:5686–93.
[24] Yang Y, Zhang K, Zhang L, Hong G, Chen C, Jing H, et al. Controllable growth of type-II Dirac semimetal PtTe2 atomic layer on Au substrate for sensitive room temperature terahertz photodetection. InfoMat 2021;3:705–15.
[25] Liu J, Fang X, He F, Yin S, Lyu W, Geng H, et al. Directional conversion of a THz propagating wave into surface waves in deformable metagratings. Opt Express 2021;29:21749–62.
[26] Song Z, Chen A, Zhang J. Terahertz switching between broadband absorption and narrowband absorption. Opt Express 2020;28:2037–44.
[27] Liu X, Starr T, Starr AF, Padilla WJ. Infrared spatial and frequency selective metamaterial with near-unity absorbance. Phys Rev Lett 2010;104:207403.
[28] Duan G, Schalch J, Zhao X, Zhang J, Averitt RD, Zhang X. Analysis of the thickness dependence of metamaterial absorbers at terahertz frequencies. Opt Express 2018;26:2242–51.
[29] Barho FB, Gonzalez-Posada F, Bomers M, Mezy A, Cerutti L, Taliercio T. Surface-Enhanced Thermal Emission Spectroscopy with Perfect Absorber Metasurfaces. ACS Photonics 2019;6:1506–14.
[30] Zhang H, Guan C, Luo J, Yuan Y, Song N, Zhang Y, et al. Facile Film-Nanoctahedron Assembly Route to Plasmonic Metamaterial Absorbers at Visible Frequencies. ACS Appl Mater Interfaces 2019;11:20241–8.
[31] Chen L, Song Z. Simultaneous realizations of absorber and transparent conducting metal in a single metamaterial. Opt Express 2020;28:6565–71.
[32] Yu P, Besteiro LV, Huang Y, Wu J, Fu L, Tan HH, et al. Broadband Metamaterial Absorbers. Adv Opt Mater 2018;7.

[33] Zhou Y, Qin Z, Liang Z, Meng D, Xu H, Smith DR, et al. Ultra-broadband metamaterial absorbers from long to very long infrared regime. Light Sci Appl 2021;10:138.
[34] Palik ED. Handbook of Optical Constants of Solids. Academic; 1985.
[35] Palik ED. Handbook of Optical Constants of Solids. Academic; 1998.
[36] Smith DR, Schultz S, Markoš P, Soukoulis CM. Determination of effective permittivity and permeability of metamaterials from reflection and transmission coefficients. Phys Rev B 2002;65.
[37] Smith DR, Schurig D. Electromagnetic wave propagation in media with indefinite permittivity and permeability tensors. Phys Rev Lett 2003;90:077405.
[38] Smith DR, Vier DC, Koschny T, Soukoulis CM. Electromagnetic parameter retrieval from inhomogeneous metamaterials. Phys Rev E: Stat Nonlinear Soft Matter Phys 2005;71:036617.
[39] Barnes WL, Dereux A, Ebbesen TW. Surface plasmon subwavelength optics. Nature 2003;424:824–30.
[40] Xu X, Li Y, Wang B, Zhou Z. Prediction of multiple resonance characteristics by an extended resistor-inductor-capacitor circuit model for plasmonic metamaterials absorbers in infrared. Opt Lett 2015;40:4432–5.

Xiaoyan shi[a,b,c,1], Enzhu Hou[a,1], Zhongzhu Liang[a,b,c,*], Shoutao Zhang[a], Rui Dai[a], Wei Xin[a], Dejia Meng[b], Hua Liu[a], Haiyang Xu[a], Yichun Liu[a]

[a] *Center for Advanced Optoelectronic Functional Materials Research and Key Laboratory of UV Light-Emitting Materials and Technology of Ministry of Education, College of Physics, Northeast Normal University, Changchun 130024, China*

[b] *State Key Laboratory of Applied Optics, Changchun Institute of Optics, Fine Mechanics and Physics, Chinese Academy of Sciences, Changchun, Jilin 130033, China*

[c] *University of the Chinese Academy of Sciences, China*

[*] Corresponding author at: Center for Advanced Optoelectronic Functional Materials Research and Key Laboratory of UV Light-Emitting Materials and Technology of Ministry of Education, College of Physics, Northeast Normal University, Changchun 130024, China.
E-mail address: liangzz@nenu.edu.cn (Z. Liang).

[1] Xiaoyan Shi and Enzhu Hou have contributed equally to this work.